

Local vapor transport synthesis of zinc oxide nanowires for ultraviolet-enhanced gas sensing

This article has been downloaded from IOPscience. Please scroll down to see the full text article.

2010 Nanotechnology 21 495502

(<http://iopscience.iop.org/0957-4484/21/49/495502>)

View [the table of contents for this issue](#), or go to the [journal homepage](#) for more

Download details:

IP Address: 169.229.32.138

The article was downloaded on 23/11/2010 at 19:07

Please note that [terms and conditions apply](#).

Local vapor transport synthesis of zinc oxide nanowires for ultraviolet-enhanced gas sensing

Lei Luo, Brian D Sosnowchik and Liwei Lin

Department of Mechanical Engineering and Berkeley Sensor and Actuator Center, 497 Cory Hall, University of California at Berkeley, Berkeley, CA 94720, USA

Received 7 July 2010, in final form 21 September 2010

Published 19 November 2010

Online at stacks.iop.org/Nano/21/495502

Abstract

A novel local vapor transport technique via induction heating is presented to enable selective, localized synthesis and self-assembly of nanowires, providing a simple and fast method for the direct integration of nanowires into functional devices. The single-crystalline zinc oxide (ZnO) nanowires are grown locally across the silicon-on-insulator microelectrodes within minutes, and the enhancement of gas sensing of ZnO nanowires is demonstrated under ultraviolet (UV) illumination at room temperature. Experiments indicate that when suspended nanowires are exposed to UV light, a twelve-fold increase in conductance and a near five-fold improvement in oxygen response are measured. Furthermore, the UV-enhanced transient responses exhibit a two-level photocurrent decay attributed to carrier recombination and oxygen readsorption. As such, the local vapor transport synthesis and UV-enhanced sensing scheme could provide a promising approach for the construction of miniaturized and highly responsive nanowire-based gas sensors.

(Some figures in this article are in colour only in the electronic version)

1. Introduction

Oxygen detection is important in clinical and analytical chemistry, biological and food processing, environmental monitoring, and industry operation safety [1]. Semiconducting metal oxide thin films, such as TiO₂, Ga₂O₃ and CeO₂, have been widely used as oxygen sensors because surface-adsorbed species can induce a detectable change in the conductance of the material [1–5]. However, their high operational temperature and large power consumption limit their practical usage. Alternatively, CuFeTe₂ [6] and In₂O₃ nanocrystals [7] have been developed for oxygen sensing at room temperature, but they have demonstrated low response or long recovery times, which are undesirable for sensor applications. Recently, zinc oxide (ZnO) nanomaterials, including nanowires, have been extensively studied for chemical sensing applications because of their good thermal stability, biocompatibility, and low cost [8–13]. Due to their large surface-to-volume ratio and single-crystalline structure, nanowires offer great potential to improve the sensitivity of gas sensors with the advantage of room temperature sensing and minimized power consumption.

The sensitivity and performance of gas sensing nanowire devices are further influenced by the ambient conditions and architecture, amongst other parameters. For example, ambient conditions, like ultraviolet (UV) light illumination, have been shown to change the carrier concentration and adsorbed surface species of ZnO nanowires [14–18], which influences the gas sensing capability. Likewise, a frequently employed architecture involves the assembly of nanowires on polished handle substrates for gas sensing [19]. However, this architecture imposes several inherent limitations since the devices are typically assembled randomly or by pick-and-place techniques with electrodes fabricated by electron-beam lithography, which is both time-consuming and expensive. Furthermore, it reduces the exposed nanowire surface area, which limits the maximum sensitivity of the device. Techniques have been demonstrated to confine the nanowire synthesis conditions [20, 21], though localized vapor confinement frequently involves complex reactant channeling systems [22] or low spatial uniformity [23].

In this work, a localized synthesis and self-assembly process has been employed for the rapid and direct integration of ZnO nanowires into functional devices. By spatially

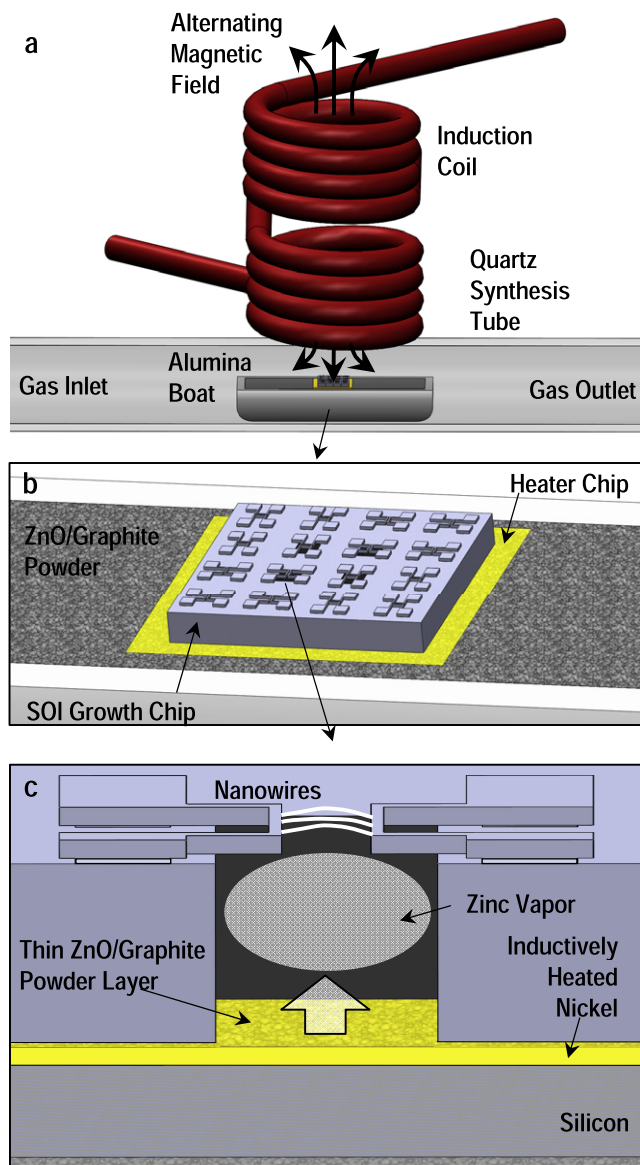


Figure 1. Setup for local vapor transport synthesis and characterization of ZnO nanowires. (a) Schematic of the induction heating setup. (b) The chip stack, consisting of a growth substrate on top of a source powder-coated heating chip. (c) Carbothermal reduction of source powder generates zinc vapor that is transported through backside etch holes for localized ZnO nanowire synthesis and self-assembly.

confining the region of generated zinc vapor using an induction heating synthesis platform [24–26], the nanowires were locally synthesized within minutes, suspended between two silicon-on-insulator (SOI) microelectrodes in an architecture exposing the entire nanowire surface area. Furthermore, the as-fabricated ZnO nanowire devices were used for oxygen sensing under different oxygen pressure environments, both in darkness and with UV illumination at 365 nm, to investigate the enhancement of oxygen response under UV illumination.

2. Experimental details

A schematic diagram of the synthesis process is shown in figure 1. Synthesis was enabled by an 11.7 MHz induction

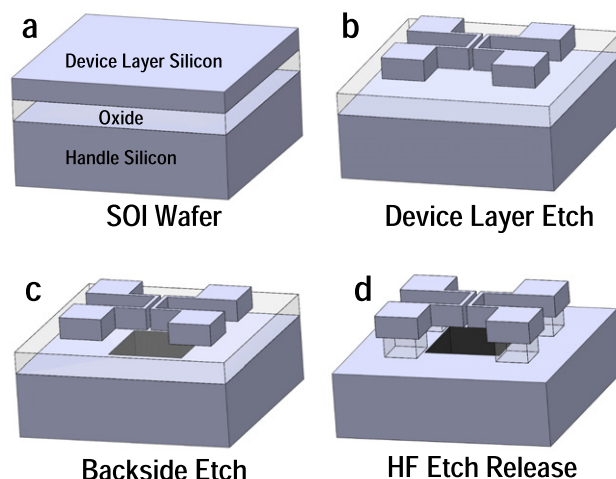


Figure 2. Process flow for the fabrication of the growth chips. (a) Silicon-on-insulator (SOI) substrates were used to create the electrodes. DRIE is used to etch both (b) the device layer and (c) the backside vapor through holes. (d) Hydrofluoric acid (HF) etching of the oxide layer releases the devices.

heating system, as shown in figure 1(a), with an eight-turn, 3.25 mm pitch, 12.7 mm inner diameter copper inductor. A chip stack, shown in figure 1(b), consisting of a growth substrate on top of a source powder-coated heating chip within an alumina boat was placed inside a quartz tube at a distance of approximately 6 mm below the base of the coil. To fabricate the growth chips, a two-mask SOI process was employed, as shown in figure 2. First, deep reactive ion etching (DRIE) was used to anisotropically etch the 50 μm thick, 5 μm -wide frontside electrodes, with $200 \times 200 \mu\text{m}^2$ contact pads separated by a distance of 10 μm . Afterward, the backside vapor through holes were DRIE etched through the 500 μm thick handle silicon, after which the devices were diced and released in hydrofluoric acid. A thin layer of gold (20–30 \AA) was evaporated onto the surface to catalyze the vapor–liquid–solid (VLS) ZnO nanowire synthesis. For the heating chips, a lightly doped silicon substrate (p-type, $\langle 100 \rangle$, 500 μm thick, 15–30 $\Omega \text{ cm}$) with a 3–4 μm layer of electroplated nickel was used. The source powder consisted of equal weights of ZnO powder (99.99% purity) and graphite powder (99% purity).

The system was initiated with a power of 380 W, inducing eddy currents in the nickel layer and rapidly elevating the temperature to ~ 900 – 950°C within 30 s. Zinc vapor was generated through the carbothermal reduction of the ZnO source powder and was spatially confined to the region above the backside opening of the growth chip, as shown in figure 1(c). Synthesis occurred for 3–5 min, enabling the rapid self-assembly of ZnO nanowires localized in the region of the two microelectrodes on the growth chip.

Figure 3(a) shows a scanning electron microscope (SEM) image of the fabricated device, with nanowire lengths up to 10 μm and diameters of 50–60 nm. Nanowire synthesis was localized to the region above the vapor through hole, and the inset shows an example of the self-assembled nanowires between the electrodes. High-resolution transmission electron microscopy (HRTEM) was used to validate the structure of the

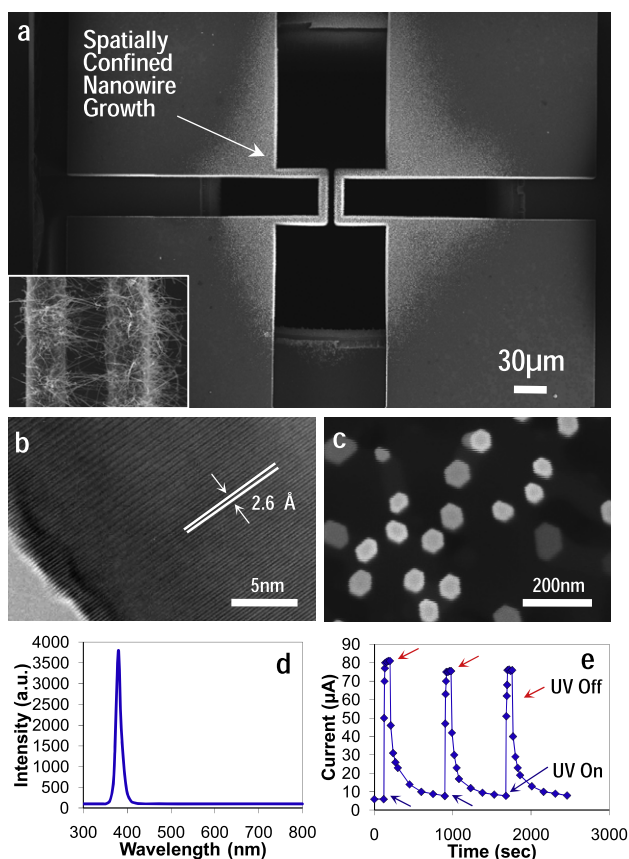


Figure 3. (a) SEM image of the fabricated device with inset showing an example of the self-assembled nanowires between the electrodes. Synthesis is isolated to the region above the vapor through hole. (b) HRTEM of the nanowire shows the lattice spacing along the ZnO(0001) direction and (c) SEM shows a hexagonal cross-section. (d) PL spectrum of the as-synthesized nanowires shows a sharp peak at 380 nm. (e) Photocurrent of ZnO nanowires at 6 V bias in ambient, room temperature conditions.

nanowire, as shown in figure 3(b). The synthesized nanowires were highly crystalline, growing along the (0001) direction with a lattice constant of 2.6 Å, and have a hexagonal cross-section, as shown in figure 3(c). The optical properties of the ZnO nanowires were investigated by photoluminescence (PL) spectroscopy at room temperature. As shown in figure 3(d), the PL spectrum presents a strong and sharp UV emission peak at ~380 nm, which was attributed to free exciton recombination corresponding to the near band-edge transition of ZnO [27]. The strong UV emission in the PL spectrum indicates that the nanowires have good crystal quality and a low concentration of defects.

Experimental measurements were performed in a stainless steel vacuum chamber using oxygen and nitrogen, both of 99.9995% purity. The chamber had a volume of approximately 463 cm³, with hermetically sealed electrical feedthroughs and a 6 mm thick glass window for external UV illumination. Data were collected using an HP 4145B semiconductor parameter analyzer and an HP 34401A digital multimeter. A 365 nm, 6 W UV lamp, positioned 20 mm above the device, was used for illumination. The penetration depth into ZnO of light at this wavelength has been reported to be ~40 nm [28], which is

comparable to the diameter of the synthesized ZnO nanowires. Therefore, appreciable light absorption is expected during the UV experiments. Furthermore, during *I*–*V* experiments under UV illumination, the device was exposed to UV radiation for at least 60 s before the *I*–*V* responses were recorded in order to ensure that the photochemical response has reached the steady state for oxygen sensing. An example of the nanowire device photocurrent with respect to time at 6 V bias is shown in figure 3(e), illustrating the reliability of the device. The sensor exhibited a twelve-fold increase in its conductance under UV illumination. Additional *I*–*V* tests (not shown) demonstrated no current flow between the electrode and the handle silicon, confirming the nanowire connection between the device layer electrodes.

3. Results and discussion

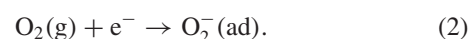
The oxygen sensing characteristics of the fabricated device were measured under various oxygen pressures. Figures 4(a) and (b) illustrate the *I*–*V* characteristics at room temperature of a ZnO nanowire device with oxygen pressures ranging from ~10³ to 10⁵ Pa in darkness and with UV illumination, respectively. The effects of oxygen and the enhanced oxygen sensitivity are observed quantitatively. First, when the gas is changed from nitrogen to oxygen, the conductance is reduced as the result of oxygen adsorption. For example, under an applied bias of 7 V in darkness and a pressure of 6.4 × 10³ Pa, the current of the device decreases from 1.75 μA in nitrogen to 1.57 μA in oxygen. Further increases of the oxygen pressure cause only small reductions in the nanowire conductance. Interestingly, an enhancement in the sensitivity to oxygen is observed with UV illumination. When changing the environment from nitrogen to oxygen at 6.4 × 10³ Pa, a 50% reduction in current flow is observed under UV illumination, compared with only a 10% current reduction without UV illumination.

Figure 4(c) quantitatively summarizes the enhanced oxygen response under UV illumination as a function of oxygen pressure. The oxygen response of the device is defined as:

$$\Delta G/G_{N_2}(\%) = \frac{100(G_{N_2} - G_{O_2})}{G_{N_2}} \quad (1)$$

where G_{N_2} and G_{O_2} are the conductances of the nanowires in a N₂ and O₂ environment, respectively. The inert nitrogen gas environment is used as the baseline reference. The enhanced oxygen response was recorded with a near five-fold improvement under UV illumination.

The mechanism behind the enhanced oxygen sensitivity is illustrated qualitatively in figure 5. It is well known that ZnO is naturally doped as an n-type semiconductor due to the oxygen vacancies and extra zinc interstitial atoms in the lattice that arise during the synthesis process [29]. Without UV illumination, oxygen molecules adsorb on the surface, capturing free electrons in the ZnO nanowire following the reaction in (2):



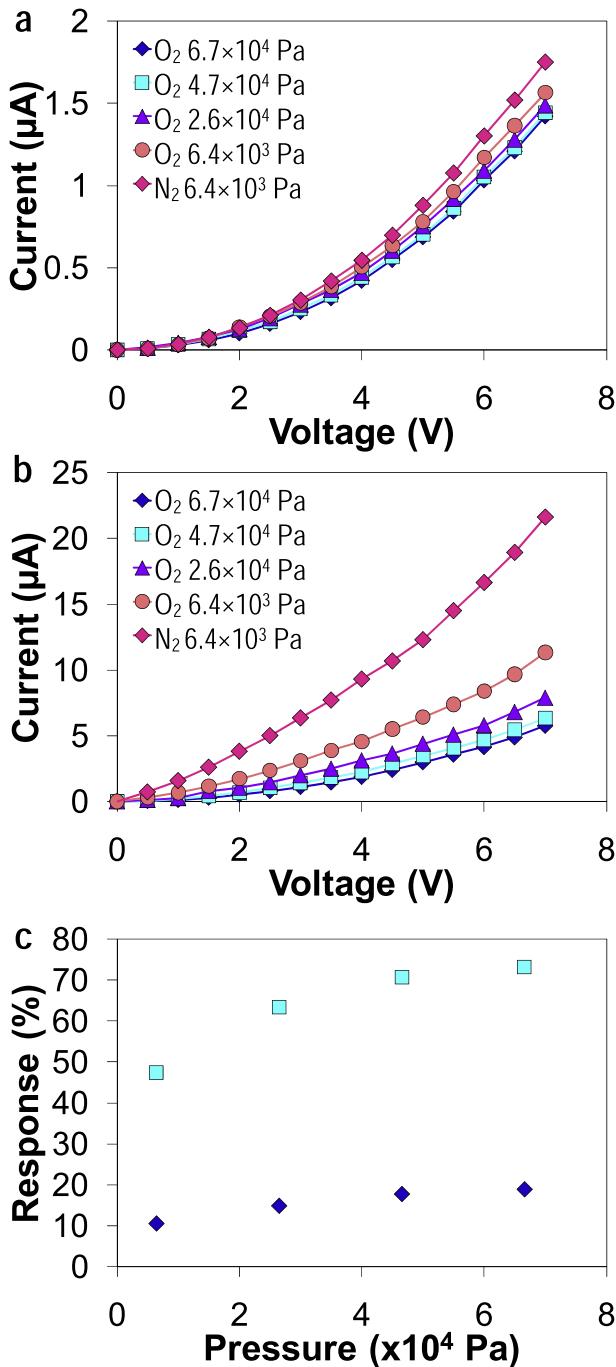


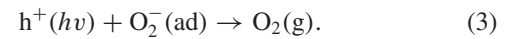
Figure 4. Current versus voltage data of a ZnO nanowire device at room temperature for various pressures of oxygen (a) in darkness and (b) with UV illumination. (c) Quantitative response to oxygen for different oxygen pressures in darkness and with UV illumination.

Both the conduction and valence bands bend near the surface, resulting in an increase in energy barrier height and a depletion layer at the surface, with a consequent reduction in the overall conductance.

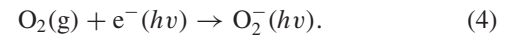
However, due to the low intrinsic carrier density and chemisorbed oxygen ions, fewer electrons are present in the nanowire, resulting in reduced sensitivity to oxygen environment change. Moreover, because of their large adsorption energy, the chemisorbed oxygen ions do not easily desorb at room temperature. This results in fewer

available surface adsorption sites for oxygen molecules, which also limits the device sensitivity. The combined effect produces smaller variations of the nanowire device conductance recorded under different oxygen pressures in dark conditions.

Conversely, under UV illumination with photon energies higher than the 3.3 eV bandgap of ZnO, electron–hole pairs are generated in the material. The photo-generated carriers lead to more electrons available to respond to the surrounding O₂ environment change. In addition, the photo-generated holes migrate to the surface along the electric field induced by the band bending and discharge chemisorbed oxygen ions following the reaction in (3):



At the same time, oxygen molecules react with the photo-generated electrons, forming photo-activated oxygen ions O₂⁻(hv) at the nanowire surface. The process occurs until the adsorption and desorption processes reach steady state following the reaction in (4) [18, 30]:



In this process, chemisorbed oxygen ions are photodesorbed from the surface, increasing the number of surface adsorption sites, and are replaced with photo-activated oxygen ions O₂⁻(hv), which have much weaker attachment to the nanowire surface and can be easily modulated under different O₂ partial pressures under UV illumination [18]. Thus, the surface concentration variation of oxygen ions is much more sensitive to the changes in the surrounding O₂ environment.

The photocurrent characteristics of the ZnO nanowire sensor under a 7 V bias at two different oxygen pressures are shown in figure 6. The photocurrent decay follows the relationship [31, 32]:

$$I(t) = I_0 \exp\left(\frac{-t}{\tau_d}\right) \quad (5)$$

where I_0 is the photocurrent before terminating the UV illumination, and τ_d is the decay time constant. Two decay time constants can be identified from the plot. The initial, rapid decay of the photocurrent, or short τ_{d1} , is due to the recombination of electrons and holes. The subsequent, slower photocurrent decay, or long τ_{d2} , is due to the slower reactions of surface re-adsorption and diffusion. As oxygen molecules gradually adsorb onto the nanowire surface and diffuse further into the nanowire for available binding sites, the carrier density is reduced slowly. From experimental results, the time constants, τ_{d1} and τ_{d2} , are calculated to be approximately 10 and 100 s, respectively, for an oxygen pressure of 6.4×10^3 Pa. When the oxygen pressure is fixed at 2.6×10^4 Pa, τ_{d1} and τ_{d2} are calculated to be 6.5 and 50 s, respectively. Decay of the photocurrent is faster under higher oxygen pressure because more oxygen is available for re-adsorption.

The as-fabricated ZnO nanowire sensor has demonstrated a higher oxygen response when compared with previous ZnO nanowire devices synthesized and assembled by other methods [19, 33, 34]. For example, three-dimensional (3D)

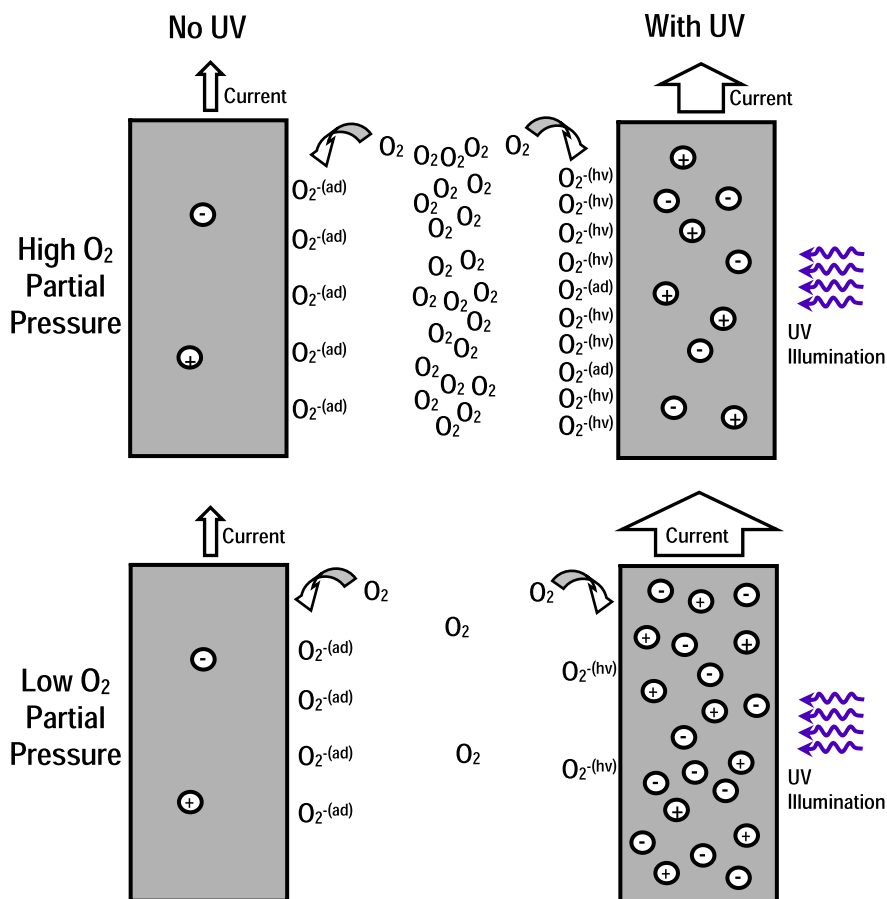


Figure 5. Mechanism behind enhanced oxygen response on ZnO nanowires. Under dark conditions, low carrier density and chemisorbed oxygen ions limit the sensitivity to O_2 . However, under UV illumination, photo-generated electron–hole pairs increase the carrier density and promote the formation of photo-activated oxygen ions, increasing the conductance and sensitivity to oxygen pressure.

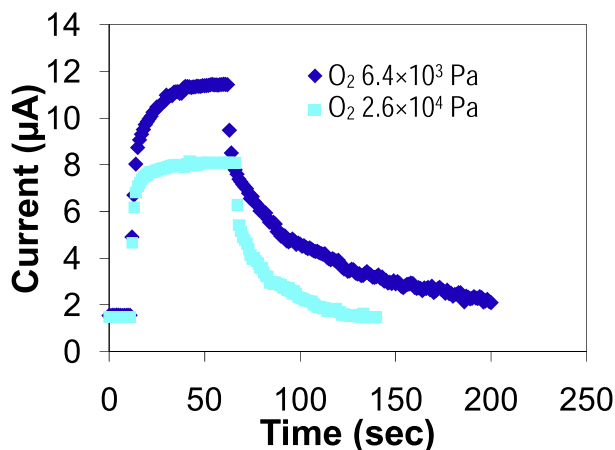


Figure 6. Expanded photocurrent illustrates two time constants from electron–hole recombination and oxygen readsorption and diffusion.

hybrid stacks, comprised of ZnO nanowire arrays, and ZnO nanowire field-effect transistors have been developed for oxygen sensing. However, the oxygen response was 17% (10% O_2) for the 3D ZnO hybrid stack [33] compared with 50% for the ZnO nanowire sensor fabricated by local vapor deposition. Also the relative conductance changes were 50%

at an O_2 pressure of 6.3×10^4 Pa and $\sim 40\%$ in ambient atmosphere (20% O_2) with a nanowire radius of 50 nm (comparable to the nanowire radius synthesized here) for single nanowire transistors lying on silicon substrates in [19, 34], which are lower than the changes observed in this work 70% and 60%, respectively. The superior performance of the as-fabricated nanowire device is attributed to the local vapor transport synthesis and assembly architecture, allowing the ZnO nanowire surface to be fully exposed, and the UV-enhanced sensing mechanism.

The performance of the ZnO nanowire sensor could be further influenced by a number of factors, including the existence of a thin native silicon dioxide layer at the interfacial contacts between the nanowire and silicon microelectrodes, the nanowire contact resistance, as well as material defects of the nanowires themselves. Future investigations to further enhance the sensitivity of the ZnO nanowire sensor include device annealing and improved contact formation.

4. Conclusion

In summary, a novel local vapor transport technique via induction heating is developed to enable selective, localized synthesis and self-assembly of ZnO nanowires for highly

responsive gas sensors. Using a backside etch process, vapor transport holes are patterned below microfabricated electrodes on an SOI wafer and confine the region of vapor generation enabling localized synthesis and self-assembly. Furthermore, the architecture exposes the entire nanowire surface for enhanced gas sensitivity. Under UV illumination a near five-fold improvement in oxygen response has been recorded, which is attributed to the increased carrier density available to respond to changes in the surrounding oxygen environment under photo-generation, and photo-activated oxygen ions $O_2^-(h\nu)$ that can be easily modulated at different oxygen partial pressures. The findings suggest that the local vapor transport synthesis and UV-enhanced sensing scheme could provide a promising approach for the realization of a new class of photochemical sensors, while the analyses and characterizations could be useful for other wide-bandgap semiconducting materials.

Acknowledgments

The authors acknowledge the UC Berkeley Microfabrication Laboratory in which test specimens were fabricated, as well as Dr Takashi Ikuno, Dr Alec Talin, and Dr Peter Yang.

References

- [1] Ramamoorthy R, Dutta P K and Akbar S A 2003 *J. Mater. Sci.* **38** 4271–82
- [2] Logothetis E M and Kaiser W J 1983 *Sensors Actuators* **4** 333–40
- [3] Ogita M, Higo K, Nakanishi Y and Hatanaka Y 2001 *Appl. Surf. Sci.* **175/176** 721–5
- [4] Fleischer M and Meixner H 1991 *Sensors Actuators B* **4** 437–41
- [5] Izu N, Shin W, Murayama N and Kanzaki S 2002 *Sensors Actuators B* **87** 95–8
- [6] Kishiro K, Kuriyaki H and Hirakawa K 1993 *Japan. J. Appl. Phys.* **32** L674–5
- [7] Neri G, Bonavita A, Micali G, Rizzo G, Galvagno S, Niederberger M and Pinna N 2005 *Chem. Commun.* **48** 6032–4
- [8] Wan Q, Li Q H, Chen Y J, Wang T H, He X L, Li J P and Lin C L 2004 *Appl. Phys. Lett.* **84** 3654–6
- [9] Chu X, Jiang D, Djurišić A B and Yu H L 2005 *Chem. Phys. Lett.* **401** 426–9
- [10] Sun Z-P, Liu L, Zhang L and Jia D-Z 2006 *Nanotechnology* **17** 2266–70
- [11] Wang J X, Sun X W, Yang Y, Huang H, Lee Y C, Tan O K and Vayssieres L 2006 *Nanotechnology* **17** 4995–8
- [12] Cheng X L, Zhao H, Huo L H, Gao S and Zhao J G 2004 *Sensors Actuators B* **102** 248–52
- [13] Liao L, Lu H B, Shuai M, Li J C, Liu Y L, Liu C, Shen Z X and Yu T 2008 *Nanotechnology* **19** 175501
- [14] Kind H, Yan H, Messer B, Law M and Yang P 2002 *Adv. Mater.* **14** 158–60
- [15] Keem K, Kim H, Kim G-T, Lee J S, Min B, Cho K, Sung M-Y and Kim S 2004 *Appl. Phys. Lett.* **84** 4376–8
- [16] Jeong M, Oh B, Lee W and Myoung J 2005 *Appl. Phys. Lett.* **86** 103105
- [17] Law J B K and Thong J T L 2006 *Appl. Phys. Lett.* **88** 133114
- [18] Fan S-W, Srivastava A K and Dravid V P 2009 *Appl. Phys. Lett.* **95** 142106
- [19] Li Q H, Liang Y X, Wan Q and Wang T H 2004 *Appl. Phys. Lett.* **85** 6389–91
- [20] Englander O, Christensen D and Lin L 2003 *Appl. Phys. Lett.* **82** 4797–9
- [21] Englander O, Christensen D, Kim J, Lin L and Morris S J S 2005 *Nano Lett.* **5** 705–8
- [22] Kometani R, Ishihara S, Kaito T and Matsui S 2008 *Appl. Phys. Express* **1** 055001
- [23] Chang P-C, Fan Z, Wang D, Tseng W-Y, Chiou W-A, Hong J and Lu J G 2004 *Chem. Mater.* **16** 5133–7
- [24] Luo L, Sosnowchik B D and Lin L 2007 *Appl. Phys. Lett.* **90** 093101
- [25] Sosnowchik B D and Lin L 2006 *Appl. Phys. Lett.* **89** 193112
- [26] Sosnowchik B D, Lin L and Englander O 2010 *J. Appl. Phys.* **107** 051101
- [27] Shan W, Walukiewicz W, Ager J W, Yu K M, Yuan H B, Xin H P, Cantwell G and Song J J 2005 *Appl. Phys. Lett.* **86** 191911
- [28] Jeong I-S, Kim J H and Im S 2003 *Appl. Phys. Lett.* **83** 2946–8
- [29] Park C H, Zhang S B and Wei S 2002 *Phys. Rev. B* **66** 073202
- [30] Barry T I and Stone F S 1960 *Proc. R. Soc. A* **255** 124–44
- [31] Zheng X G, Li Q S, Hu W, Chen D, Zhang N, Shi M J, Wang J J and Zhang L C 2007 *J. Lumin.* **122/123** 198–201
- [32] Poti B, Passaseo A, Lomascolo M, Cingolani R and Vittorio M D 2004 *Appl. Phys. Lett.* **85** 6083–5
- [33] Jeong M, Oh B, Nam O, Kim T and Myoung J 2006 *Nanotechnology* **17** 526–30
- [34] Fan Z, Wang D, Chang P, Tseng W and Lu J G 2004 *Appl. Phys. Lett.* **85** 5923–5